Systematic study of α-decay properties of superheavy nuclei

A. I. Budaca and I. Silişteanu*

Horia Hulubei National Institute of Physics and Nuclear Engineering, Bucharest-Magurele RO-077125, Romania

(Received 21 August 2013; published 28 October 2013)

The α decay of superheavy nuclei (SHN) is studied within the framework of the shell-model rate theory. The α half-lives are calculated in terms of the α clustering and resonance scattering amplitudes given by self-consistent models for the nuclear structure and reaction dynamics. The results and their systematics are compared with the available experimental data and with those data obtained from empirical models. The Brown relationship [B. A. Brown, Phys. Rev. C **46**, 811 (1992)], which predicts a linear dependence of the $\log T_\alpha$ on $Z_d^{0.6} Q_\alpha^{-1/2}$, is used to obtain a relevant systematics for α half-lives of the observed SHN. Also, simple fit formulas are proposed for α-half-time estimations with reduced standard errors. Comparison of experimental and calculated results provides insight into the accuracy of modern approaches for the structure of SHN with valence nucleons outside the doubly magic core.

DOI: 10.1103/PhysRevC.88.044618 PACS number(s): 23.60.+e, 21.10.Tg, 25.70.Jj, 27.90.+b

I. INTRODUCTION

For superheavy nuclei (SHN) located far away from the β-stability line on the proton-rich side, the binding energy rapidly decreases, due to increasing Coulomb repulsion and reaction Q values, which leads to two major difficulties with regard to both SHN production in fusion-evaporation reactions and the study of their decay properties. The first difficulty is related to the fact that large Q values imply high excitations in the involved nuclear systems. The second one is a consequence of the first, meaning that large Q values open up many decay channels favoring the nuclei closer to stability.

Both the amount and quality of experimental data on the nuclear energy levels and the decay modes of SHN have increased considerably in the last few years [1–15]. The decay data reveal that for SHN the dominant decay mode is α emission, not fission.

The SHN have now become available for experimental studies with in-beam and decay spectroscopic methods [1,8,16] and also for systematic studies through phenomenological and theoretical approaches [17–21]. These detailed investigations provide the access to the basic properties of SHN: masses, energy levels, lifetimes, spins, moments, reaction energies, and emission rates. Moreover, α decay has become a powerful tool to explore the nuclear structure (α clustering, fine structure, shell effects, and deformation) and also to reveal the most important aspects of reaction mechanisms (resonance tunneling, phase transitions, and channel coupling).

The α decay of SHN has yielded much energy level information for nuclear spectroscopy and it is one of the most useful probes for studying the structure of SHN [22]. Studies of production and decay of SHN are revealing new competing decay modes and complex nuclear structures involving weakly bound states coupled to an environment of scattering states. The main features of the nuclear structure can be revealed by observing the evolution of basic quantities that characterize the nucleus [23]. There have been several efforts to correlate the existing α-decay data on an empirical basis to give insight into the nature of the process. However, it is difficult to correlate data with the evolution of nuclear structure observables.

In the present work, our aim is to correlate on a theoretical basis the measured reaction energies E_α with the microscopic information on nuclear structure to make reasonable predictions for the emission rates, i.e., the α half-lives, T_α, and the decay widths, Γ_α. Theoretical results are confronted with the available experimental data and the results of other relevant approaches to obtain the net contributions of the shell structure, finite size, and screening effects to the emission rates. Also, we compare the systematics of experimental ($T_\alpha^{\rm exp}$, $Q_\alpha^{\rm exp}$) and shell-model (SM) results ($T_\alpha^{\rm SM}$, $Q_\alpha^{\rm exp}$) to discuss possible sources for some large discrepancies between experiment and theory.

This paper is organized as follows. In Sec. II the formalism is briefly reviewed. In Sec. III the results for the α half-lives, the systematics of the α-decay properties for almost all the known SHN at the present date, and the fit formulas for practical estimations of α half-lives are presented. The concluding remarks are summarized in Sec. IV.

II. SHELL-MODEL RATE THEORY

For studying the essential features of α decay of SHN we use the shell-model rate theory (SMRT) [24]. The SMRT unifies the advantages of the microscopic description of the α-particle preformation process [25] with the ones of the theory of resonance reactions [26,27] in describing the reaction dynamics. Apart from the R-matrix theory which contains the channel radius as an arbitrary parameter, the SMRT is free from the parameters of the theory. The procedure is to smoothly match the four shell-model (SM) wave functions of individual nucleons ($I_n^{k[\rm SM]}(r)$ which describe the SM formation amplitude of the outgoing α- particle (in channel n from the resonance state k) with a general solution of the

*silist@theory.nipne.ro

 ©2013 American Physical Society

system of differential equations:

$$\left[\frac{\hbar^2}{2m}\left(\frac{d^2}{dr^2}-\frac{l(l+1)}{r^2}\right)-V_{nn}(r)+Q_n\right]u_n^0(r) + \sum_{m\neq n}V_{nm}(r)u_m^0(r)=0, \quad (1)$$

$$\left[\frac{\hbar^2}{2m}\left(\frac{d^2}{dr^2}-\frac{l(l+1)}{r^2}\right)-V_{nn}(r)+Q_n\right]u_n^k(r) + \sum_{m\neq n}V_{nm}(r)u_m^k(r)=I_n^{k[\mathrm{SM}]}(r). \quad (2)$$

These equations define an α particle of a given kinetic energy, Q_α, and an angular momentum, l, moving in the potential $V_{nm}(r)$. The solutions of the above system represent the radial motion of the fragments at large and small separations, respectively, in terms of the reduced mass of the system m, the kinetic energy of the emitted particle $Q_\alpha = Q_n = E - E_D - E_\alpha$, the formation amplitude (FA) $I_n^k(r)$, and the matrix elements of the interaction potential $V_{nm}(r)$.

The effective decay energy used in the above relations is

$$Q_\alpha = \frac{A}{A-4}E_\alpha^{\mathrm{exp}} + \left(6.53Z_d^{7/5} - 8.0Z_d^{2/5}\right)10^{-5}, \quad (3)$$

where A is the mass number of the parent nucleus, E_α^{exp} is the measured kinetic energy of the α particle, and the second term is the screening correction [28].

The matrix elements $V_{nm}(r)$ include nuclear and Coulomb components [29] defined with the quadrupole (β_2) and hexadecapole (β_4) deformation parameters of the daughter nucleus [30]. To avoid the usual ambiguities encountered in formulating the potential for the resonance tunneling of the barrier we iterate directly the nuclear potential in the equations of motion [29,31].

The SM α-particle FA is defined as the antisymmetrized projection of the parent wave function on the channel wave function:

$$I_n^{k[\mathrm{SM}]}(r) = r\left\langle \Psi_k^{\mathrm{SM}}(r_i)\middle|\mathcal{A}\left\{\left[\Phi_D^{\mathrm{SM}}(\eta_1)\Phi_p(\eta_2)Y_{lm}(\hat{r})\right]_n\right\}\right\rangle, \quad (4)$$

where $\Phi_D^{\mathrm{SM}}(\eta_1)$ and $\Phi_\alpha(\eta_2)$ are the internal (space-spin) wave functions of the daughter nucleus and of the particle, $Y_{lm}(\hat{r})$ is the wave function of the angular motion, $\mathcal{A}$ is the inter-fragment antisymmetrizer, r connects the centers of mass of the fragments, and the symbol $\langle\,|\,\rangle$ means integration over the internal coordinates and the angular coordinates of the relative motion. It should be pointed out that the spatial correlations imposed by the Pauli principle on the nucleons in a simple SM configuration are sufficient to determine the essential features of nuclear motion in the preformation stage.

Following Ref. [25] we use in Eq. (4) the wave functions (WFs) $|\Psi_k^{\mathrm{SM}}(r_i)\rangle = \det\|\psi_{nlj}^{\mathrm{SM}}(r_i)\|$, $i = 1, A$, and $|\Phi_D^{\mathrm{SM}}\rangle = \det\|\psi_{nlj}^{\mathrm{SM}}(\eta_{1i})\|, i = 1, A-4$, where $\psi_{nlj}^{\mathrm{SM}}(r_i)$ are the standard nuclear SM single-particle WFs [32], and the α-particle WF

$$\Phi_\alpha(\eta_2) = (2/(1/2)!)^{3/2}(\beta/\pi)^{9/4}\left(\rho_1^2+\rho_2^2+\rho_3^2\right) \times (4\pi)^{-3/2}\chi_{00}(s_1s_2)\chi_{00}(s_3s_4), \quad (5)$$

where the α-particle oscillator parameter is $\beta = 0.484$ fm^{-2}, χ_{00} is the singlet spin function, and the internal spatial coordinates $\rho_1 = (r_1 - r_2)/\sqrt{2}$, $\rho_2 = (r_3 - r_4)/\sqrt{2}$, and $\rho_3 = (r_1 + r_2 - r_3 - r_4)/2$ are connected to the individual coordinates r_i of the four nucleons. To perform the integrations in Eq. (4) we need to transform the WF $\Psi_k^{\mathrm{SM}}(r_i)$ from the individual coordinates $(r_i) \longrightarrow r$, η_1, and η_2 to the center-of-mass system coordinate r and internal coordinates η_1 and η_2 of the fragments. Further, by integrating over the internal coordinates and the angular coordinates of the relative motion of fragments, the overlap integral is easily obtained.

For nuclei with $Z = 102$–120 we use single-proton states [32]: $1i_{13/2}, 2f_{7/2}, 2f_{5/2}, 3p_{3/2}, 3p_{1/2}$; and for nuclei with $N = 150$–178 we use single-neutron states: $2g_{9/2}, 2g_{7/2}, 3d_{5/2}, 3d_{3/2}, 4s_{1/2}$.

The α-decay width is given by

$$\Gamma_n^{k[\mathrm{SM}]} = 2\pi\left|\frac{\int_{r_{\mathrm{min}}}^{r_{\mathrm{max}}} I_n^{k[\mathrm{SM}]}(r)u_n^0(r)dr}{\int_{r_{\mathrm{min}}}^{r_{\mathrm{max}}} I_n^k(r)u_n^{k[\mathrm{SM}]}(r)dr}\right|^2, \quad (6)$$

where the lower limit in the integrals is an arbitrary small radius, $r_{\mathrm{min}} > 0$, while the upper limit r_{max} is close to the first exterior node of $u_n^0(r)$.

The α half-life is expressed as

$$T_n^{k[\mathrm{SM}]} = \ln 2\frac{\hbar}{\Gamma_n^{k[\mathrm{SM}]}}. \quad (7)$$

The α half-lives derived from Eqs. (8) and (7) depend on the nuclear single-particle wave functions and finite sizes of nucleons and α particles (see Ref. [25] for details). Also these half-lives include the correction terms due to screening and resonance scattering effects.

Finally, the SM half-lives are corrected by the even-odd terms h_{e-o} extracted from the available decay data (see Sec. III):

$$\log T_n^{k[\mathrm{SM}]}(s) \Longrightarrow \log T_n^{k[\mathrm{SM}]}(s) + h_{e-o}. \quad (8)$$

III. RESULTS AND DISCUSSION

A. α half-lives

Nuclei with the atomic number $Z = 102$–118 (including even-even, even-odd, odd-even, and odd-odd species) taken into account in the present calculations are shown in Table I together with emission energies. These nuclides decay primarily through α emission ($T_\alpha < T_{\mathrm{SF}}$). The decay chains of consecutive α emissions are terminated by the spontaneous fission (SF) ($T_\alpha > T_{\mathrm{SF}}$).

The results for the α half-lives obtained from Eqs. (1)–(8), using only experimental emission energies [1–15], are presented in column 6 of Table I. In column 7 are shown the results of a linear fit of the SM half-lives T_α^{fit} (see Sec. III C).

With regard to Table I we would like to reveal the following:

(i) a considerable increase of α half-lives with an increasing number of neutrons in all isotopic sequences;
(ii) a decrease of α half-lives with an increasing number of protons in isotonic sequences;
(iii) the prominent α emitters are very neutron-deficient isotopes with the α half-lives in the range of about 10^{-6}–10^{-5} s to 1–2 min;

TABLE I. Experimental [1–3,5,9–12,33] and calculated α-decay properties of the measured SHN.

Nucleus	$l_{\min}$	$E_\alpha^{\exp}$	Q_α	$\log T_\alpha^{\exp}$	$\log T_\alpha^{\mathrm{SM}}$	$\log T_\alpha^{\mathrm{fit}}$
^{251}No	0	8.620	8.801	−0.119	0.790	0.981
^{253}No	0	8.010	8.181	1.982	2.954	3.010
^{254}No	0	8.100	8.271	1.708	1.575	3.576
^{255}No	0	8.120	8.291	2.270	2.577	2.632
^{256}No	0	8.450	8.626	0.464	0.406	2.386
^{257}No	0	8.340	8.514	1.398	1.834	1.894
^{259}No	0	7.680	7.842	3.542	4.167	4.215
^{254}Lr	0	8.460	8.638	1.114	1.849	1.824
^{255}Lr	0	8.430	8.607	1.338	1.608	1.924
^{256}Lr	0	8.520	8.698	1.431	1.657	1.633
^{257}Lr	0	8.860	9.043	−0.187	0.245	0.572
^{258}Lr	1	8.650	8.829	0.613	1.243	1.223
^{259}Lr	0	8.440	8.615	0.792	1.582	1.898
^{260}Lr	0	8.040	8.208	2.255	3.288	3.253
^{255}Rf	0	8.770	8.953	0.204	1.166	1.165
^{257}Rf	0	9.020	9.206	0.672	0.401	0.409
^{259}Rf	0	8.890	9.072	0.519	0.802	0.803
^{261}Rf	0	8.280	8.452	1.833	2.638	2.760
^{256}Db	0	9.010	9.197	0.230	0.826	0.752
^{257}Db	0	9.160	9.348	−0.097	0.034	0.310
^{258}Db	0	9.170	9.358	0.643	0.350	0.282
^{259}Db	0	9.470	9.662	−0.292	−0.862	−0.570
^{260}Db	1	9.120	9.306	0.176	0.502	0.432
^{261}Db	0	8.930	9.113	0.255	0.737	1.001
^{262}Db	0	8.670	8.848	1.544	1.903	1.810
^{263}Db	0	8.360	8.533	1.462	2.589	2.822
^{259}Sg	0	9.620	9.815	−0.319	−0.656	−0.679
^{260}Sg	0	9.810	10.007	−2.444	−2.241	−0.392
^{261}Sg	0	9.560	9.753	−0.638	−0.485	−0.511
^{263}Sg	0	9.250	9.437	−0.523	0.412	0.368
^{265}Sg	0	8.830	9.010	0.851	1.703	1.630
^{266}Sg	0	8.630	8.806	1.531	1.282	3.132
^{269}Sg	0	8.570	8.744	2.108	2.406	2.462
^{271}Sg	0	8.540	8.712	2.057	2.654	2.563
^{261}Bh	0	10.400	10.607	−1.928	−2.688	−2.395
^{262}Bh	0	10.370	10.576	−2.097	−2.270	−2.319
^{264}Bh	1	9.620	9.813	−0.356	−0.270	−0.369
^{266}Bh	1	9.290	9.477	0.230	0.686	0.565
^{267}Bh	1	8.830	9.009	1.230	1.765	1.949
^{270}Bh	1	8.930	9.109	1.785	1.655	1.644
^{271}Bh	1	9.350	9.535	0.079	0.045	0.400
^{272}Bh	3	9.150	9.331	1.079	0.983	0.984
^{274}Bh	3	8.800	8.975	1.733	2.214	2.054
^{263}Hs	0	10.900	11.114	−0.131	−3.408	−3.289
^{264}Hs	0	10.430	10.636	−3.585	−3.221	−1.397
^{265}Hs	0	10.570	10.777	−3.097	−2.503	−2.512
^{266}Hs	0	10.180	10.381	−2.638	−2.577	−0.758
^{267}Hs	0	9.880	10.076	−1.481	−0.708	−0.767
^{269}Hs	0	9.230	9.415	0.987	1.164	1.051
^{270}Hs	0	8.880	9.059	1.362	1.045	3.201
^{271}Hs	0	9.140	9.322	0.602	1.304	1.321
^{273}Hs	0	9.590	9.778	−0.620	−0.017	0.029
^{275}Hs	0	9.300	9.483	−0.721	0.962	0.856
^{266}Mt	0	11.740	11.965	−2.769	−4.843	−4.834
^{268}Mt	0	10.240	10.441	−1.155	−1.303	−1.405
^{270}Mt	0	10.030	10.227	−0.086	−0.743	−0.863
^{274}Mt	1	10.020	10.214	−0.485	−0.831	−0.831
^{275}Mt	0	10.330	10.528	−1.921	−1.984	−1.622
^{276}Mt	0	9.710	9.899	−0.143	0.150	0.002
^{278}Mt	0	9.550	9.735	0.716	0.482	0.449
^{267}Ds	0	11.600	11.823	−5.523	−4.306	−4.268
^{269}Ds	0	11.110	11.324	−3.770	−3.197	−3.197
^{270}Ds	0	11.000	11.212	−4.000	−4.111	−2.185
^{271}Ds	0	10.740	10.947	−2.959	−2.308	−2.339
^{273}Ds	0	11.200	11.413	−3.770	−3.401	−3.393
^{277}Ds	0	10.570	10.771	−2.245	−1.990	−1.923
^{279}Ds	0	9.700	9.888	−0.699	0.463	0.331
^{281}Ds	0	8.730	8.903	1.301	3.316	3.230
^{272}Rg	0	10.820	11.029	−2.824	−2.153	−2.245
^{274}Rg	0	11.150	11.362	−2.194	−2.942	−3.003
^{278}Rg	0	10.690	10.893	−2.367	−1.939	−1.928
^{279}Rg	0	10.370	10.568	−0.770	−1.347	−1.141
^{280}Rg	0	9.750	9.938	0.556	0.696	0.491
^{282}Rg	0	9.180	9.359	1.602	2.264	2.136
^{277}Cn	0	11.450	11.666	−3.155	−3.392	−3.389
^{281}Cn	0	10.310	10.507	−1.013	−0.706	−0.700
^{283}Cn	0	9.540	9.725	0.580	1.595	1.381
^{285}Cn	0	9.150	9.328	1.462	2.804	2.535
^{278}Uut[a]	2	11.680	11.899	−3.620	−3.578	−3.613
^{282}Uut[a]	0	10.620	10.821	−1.210	−1.156	−1.189
^{283}Uut[a]	0	10.120	10.313	−1.000	−0.042	0.082
^{284}Uut[a]	0	9.970	10.161	−0.013	0.586	0.483
^{285}Uut[a]	0	9.740	9.927	0.738	1.041	1.114
^{286}Uut[a]	2	9.630	9.815	1.293	1.709	1.425
^{286}Fl	0	10.180	10.373	−0.886	−0.659	1.042
^{287}Fl	0	10.020	10.211	−0.319	0.854	0.642
^{288}Fl	0	9.950	10.080	−0.097	0.019	1.699
^{289}Fl	0	9.820	10.007	0.415	1.433	1.190
^{287}Uup[a]	0	10.590	10.789	−1.456	−0.683	−0.548
^{288}Uup[a]	0	10.480	10.677	−1.060	−0.049	−0.271
^{289}Uup[a]	0	10.500	10.697	−0.420	−0.571	−0.320
^{290}Uup[a]	2	10.200	10.392	−0.620	0.584	0.453
^{290}Lv	0	10.840	11.042	−2.167	−1.799	−0.076
^{291}Lv	0	10.740	10.940	−1.699	−0.473	−0.635
^{292}Lv	0	10.660	10.858	−1.397	−1.328	0.376
^{293}Lv	0	10.540	10.736	−1.097	0.057	−0.136
^{293}Uus[a]	0	11.030	11.233	−1.569	−1.209	−1.056
^{294}Uus[a]	0	10.810	11.010	−1.108	−0.302	−0.527
^{294}Uuo[a]	0	11.650	11.862	−3.046	−3.198	−1.422
^{295}Uuo[a]	0	11.550	11.760	−3.000	−1.895	−1.976
^{298}Ubn[a]	0	12.400	12.621	−4.523	−4.336	−2.497
^{299}Ubn[a]	0	12.300	12.519	−4.301	−3.050	−3.048

[a]Temporary names assigned according to the convention of *the systematic element names*.

(iv) the half-lives of even-even nuclei are always shorter than the half-lives of their neighbors even-odd, odd-even, and odd-odd nuclei;

(v) there are also significant differences between the half-lives of nuclei with an identical number of additional nucleons (or α particles) and the ones with an identical number of nucleon (or α particle) holes in doubly magic cores and of $Z = 108$, $N = 162$, and $Z = 114$, and N approaching 184.

The differences mentioned at the last two points are connected with the pairing interaction and the α periodicity of nuclear properties which are manifested in heavy and superheavy nuclei. These differences are illustrated graphically in Sec. III C.

An example concerning the last point above is the doubly magic deformed nucleus ^{270}Hs from the α-decay chain ^{274}Ds(^{270}Hs+α) $\rightarrow$ ^{270}Hs $\rightarrow$ ^{266}Sg(^{270}Hs$-\alpha$). Notice that, the nuclide ^{274}Ds is not yet observed and our prediction for its α half-life is about $10^{-4} - 10^{-5}$ s. The α half-lives of successive daughter nuclei increase so that we have $T_\alpha(^{274}\text{Ds}) \ll T_\alpha(^{270}\text{Hs}) < T_\alpha(^{266}\text{Sg})$. Similar α-decay channels and experimental and theoretical SM values for α half-lives are well known for the the spherical doubly magic ^{208}Pb and ^{100}Sn nuclei [24]:

^{212}Po(^{208}Pb+α) $\rightarrow$ ^{208}Pb $\rightarrow$ ^{204}Hg(^{208}Pb$-\alpha$);
^{104}Te(^{100}Sn+α) $\rightarrow$ ^{100}Sn.

In other words, nuclei from unstable configurations undergo spontaneous α decay until stability is reached. As has been noted in Ref. [21], the SM results are very sensitive to the assignment of the single proton and neutron states. Thus, the α half-time for the decay of ^{286}Fl agrees well with the observed data if the parent configuration is $2[2f_{7/2}]_p, 2[2g_{7/2}]_n$, whereas another configuration leads to a wrong result. In the same way the meta-stable high-spin states [12] can be uniquely determined by a precise configuration that reproduces the experimental data on the α-decay data of the isomeric state, with other configurations leading to wrong results.

In general, the α half-lives presented in Table I are in a good agreement with most of the updated α-decay data [33] and also with some calculated results [34]. The agreement with the predictions of the different models [17–20] is also good, if these include the same additional corrections for screening and even-odd effects. Notice that for a number of nuclei the values T_α^{exp} are only estimates with the Viola-Seaborg formula [Eq. (B1)] using experimental emission energies. The appropriate results of different models show that the essential factor determining α half-lives is the emission energy. However, for a few nuclei, ^{266}Mt, ^{281}Ds, and ^{282}Rg, we observe large differences between theory and experiments, see Table II. Such discrepancies of about 2 or 3 orders of magnitude, we have assumed [21,22] to arise from possible measurement errors. Even recently, a new series of experiments has been performed to obtain more detailed information on the decay properties of odd-Z nuclei as well as to measure the excitation functions of the ^{243}Am + ^{48}Ca and ^{249}Bk + ^{48}Ca reactions at a more extended range of projectile energies and to verify the reported discoveries of elements 113, 115, and 117 [1]. Several new

TABLE II. Superheavy nuclei with large discrepancies between calculated and experimental half-lives.

Nucleus	E_α^{exp}	Q_α	$\log T_\alpha^{\text{exp}}$	$\log T_\alpha^{\text{SM}}$	$\log T_\alpha^{\text{VS}}$	$\log T_\alpha^{B}$
^{263}Hs	10.900	11.114	–0.131	–3.408	–3.405	–2.874
^{266}Mt	11.740	11.965	–2.770	–4.843	–4.937	–4.198
^{281}Ds	8.730	8.903	1.301	3.316	3.321	2.914

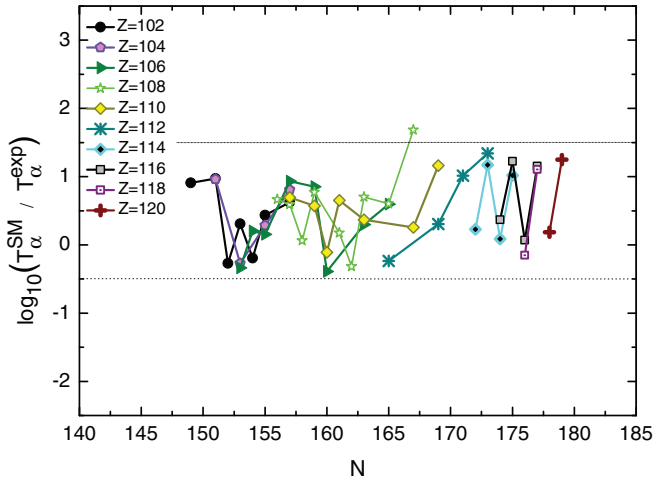

FIG. 1. (Color online) Logarithm of $T_\alpha^{\text{SM}}/T_\alpha^{\text{exp}}$ vs the neutron number N for the heaviest nuclei with $Z = 102$–120, Z-even. These values are distributed around the value 0.5 of the logarithm, which corresponds to the absolute deviations of the half-lives with a factor of 3.2.

data are in much better agreement with our predictions for ^{282}Rg and ^{290}Uup nuclei than the previous measured values. A special case would be ^{281}Ds, which is known to decay only by spontaneous fission [4]. However Düllmann *et al.* [12] report also the existence of an α-decay branch I_α of 9^{+16}_{-7}% for this nucleus, which we take into account in our calculations.

For further insight, we give a comparison of the calculated results with the experimental data for isotopes of different elements (Figs. 1 and 2). One can see that the absolute values of $\log(T_\alpha^{\text{SM}}/T_\alpha^{\text{exp}})$ are generally less than 1.5.

In Figs. 1 and 2 are plotted the deviations of even-Z ($Z = 102$–120) and odd-Z ($Z = 103$–117) isotopes versus the proton number of the parent nucleus. From these figures one can see that the deviation of $T_\alpha^{\text{SM}}/T_\alpha^{\text{exp}}$ decreases from

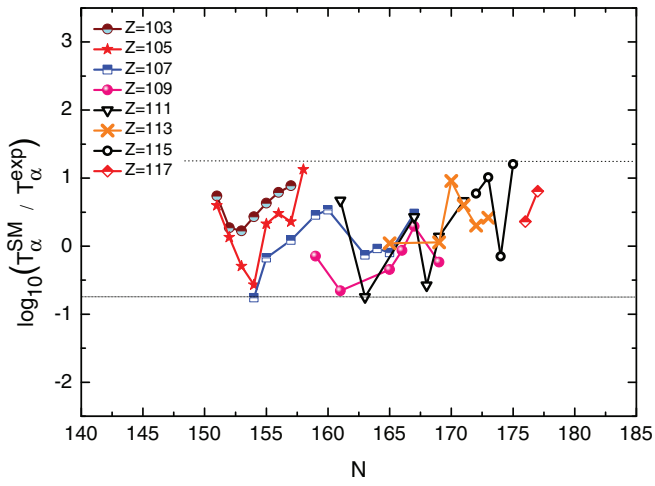

FIG. 2. (Color online) Logarithm of $T_\alpha^{\text{SM}}/T_\alpha^{\text{exp}}$ vs the neutron number N for the heaviest nuclei with $Z = 102$–120, Z-odd. These values are distributed around the value 0.25 of the logarithm, which corresponds to the absolute deviations of the half-lives with a factor of 1.8.

the neutron number $N = 151$ for several isotopic chains. This is due to the influence of the spherical shell closure. Similarly, one can see that the deviations generally decrease with the neutron number approaching the deformed $N = 162$ ($Z = 108$) shell and moving away from the spherical shell closure. We used the property of this ratio to point out the theoretical shortcomings made in Ref. [35] but only for heavy nuclei and several SHN.

The structural characteristics of SHN change rather smoothly for two neighboring nuclei but isolated jumps in their α half-lives appear only for transitions across major shells. The α half-lives are strongly modulated by major shell effects, leading to very short α half-lives above and long α half-lives below the magic shells.

For the 99 even-even, odd-even, even-odd, and odd-odd SHN, the value of the standard deviation is 0.65, which is defined as

$$\sqrt{\langle \sigma^2 \rangle} = \sqrt{\frac{1}{N}\sum_{i=1}^{N}\left(\log T_\alpha{}^{\mathrm{SM}} - \log T_\alpha^{\mathrm{exp}}\right)^2}.$$

Such a value (0.65) corresponds to a relative mean factor of 4.43 between the theoretical (T_α^{SM}) and experimental half-lives, which is a relatively good agreement. It is important to achieve good agreement for the α half-lives predicted by the fits of the microscopic and macroscopic α half-lives (shown in Figs. 5 and 9), because in both fits the structure factor is represented by a free constant.

B. Systematics of α half-lives

First, we verify the empirical Brown ($\log T_\alpha Z_d^{0.6} Q_\alpha^{-1/2}$) and Geiger-Nuttall ($\log T_\alpha \sim Q_\alpha^{-1/2}$) relationships, which predict a linear dependence of $\log T_\alpha$ vs $Z_d^{0.6} Q_\alpha^{-1/2}$ and $Q_\alpha^{-1/2}$ for the measured α half-lives. Second, such a linear dependence, which is revealed by the calculated α-decay half-lives, constitutes a starting point in the systematics of α-decay properties.

The first systematics of α-decay lifetimes of natural emitters was obtained by plotting the experimental values of $\log T_\alpha^{\mathrm{exp}}$ vs $Q_\alpha^{-1/2}$ [36]. Figure 3 shows a version of this plot for the ground state to ground state α-decay half-lives of the known SHN for the experimental data. In such a plot the points are distributed on roughly straight lines (for the element Z_d) and the deviation of data from these lines is given by the *rms* value. Other similar relations have been proposed which contain the same energy dependence but different powers of Z_d [37,38]. Further, as previously noted in Ref. [38], the dependence $\log T_\alpha$ vs $Z_d Q_\alpha^{-1/2}$ shown in Fig. 4 may be a better way to plot the data because in this case the data points are also ordered over the Z_d values and the scatter is less pronounced than in the dependence $\log T_\alpha$ vs $Q_\alpha^{-1/2}$ (see Fig. 3). The best linear fit is obtained when $\log T_\alpha$ values are plotted vs $Z_d^{0.6} Q_\alpha^{-1/2}$, as shown in Fig. 5. In fact, Eq.(B2), i.e., $\log T_\alpha$ vs. $Z_d^{0.6} Q_\alpha^{-1/2}$ appears as a simple interpolation between the plots $\log T_\alpha$ vs $Q_\alpha^{-1/2}$ and $Z_d Q_\alpha^{-1/2}$ for which the rms values has a sharp minimum. Although this dependence does not have a physical interpretation, it also came out numerically from the Wentzel-Kramers-Brillouin (WKB) calculations performed

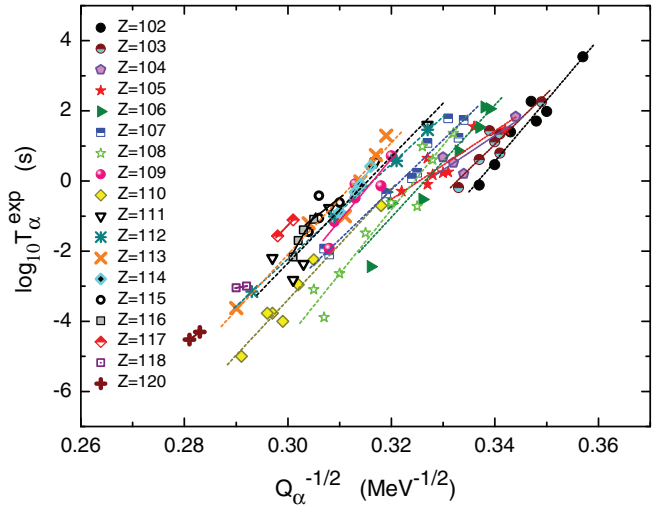

FIG. 3. (Color online) The experimental α half-lives plotted vs $Q_\alpha^{-1/2}$ for 99 data points.

by Brown [38]. The half-lives were calculated using the semiclassical approximation of the decay rate $T_\alpha = \frac{1}{W}$, with $W = P W_c T$, where P is the preformation probability, W_c is the collision rate of the α particle with the nuclear surface, and T is the barrier penetration factor defined within the WKB approximation. The numerical results for $\log \frac{1}{W}$ plotted as function of $Z_d^{0.6} Q_\alpha^{-1/2}$ were found to follow the straight line dependence even better than the fit of the data for nuclei with $Z_d = 74$–106. It is obvious that such a dependence is not bound to the used theoretical description, but rather to the general property of the α decay. This fact is also supported by the present results, where a similar linear dependence was obtained by means of a microscopic formalism. Indeed, in Ref. [38], the analysis of 119 data points (T_α, Q_α) showed that $\log T_\alpha$ vs $Z_d^{0.6} Q_\alpha^{-1/2}$ is a better way to plot the data to identify the specific behavior of each decay chain. Although this systematics pointed out evident regularities in the $\log T_\alpha$

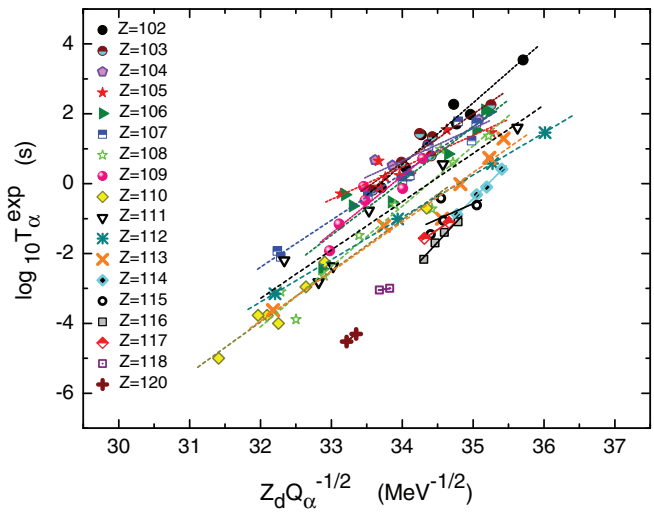

FIG. 4. (Color online) The experimental α half-lives plotted vs $Z_d Q_\alpha^{-1/2}$ for 99 data points.

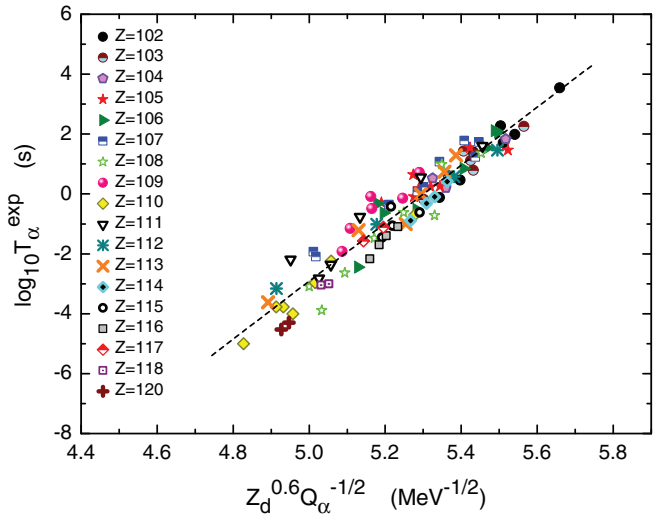

FIG. 5. (Color online) The experimental α half-lives plotted vs $Z_d^{0.6} Q_\alpha^{-1/2}$ for 99 data points. The straight line represents the result of the single-line linear fit.

vs $Z_d^{0.6} Q_\alpha^{-1/2}$ representation of the nuclei known until 1992, it doesn't contain the odd-A and odd-odd nuclei, for which an additional even-odd correction term h_{e-o} is needed. Thus, we added this correction in all the methods employed in the present study, except the Viola-Seaborg formula, which has this correction already included by default.

In the Brown-type plot, i.e., $\log T_\alpha$ vs $Z_d^{0.6} Q_\alpha^{-1/2}$, we represent the experimental and calculated SM α half-lives for all (e-e) and (e-o, o-e, o-o) nuclei. The results are shown in Figs. 5, 6, 9, and 10.

For SHN, an uncertainty in the l values of current experimental data arises [7], since α-decay either to ground and excited states or from isomeric states is allowed for both $l = 0$ and $l \neq 0$ transitions. The values and scatter of $\log T_\alpha^{\exp}$

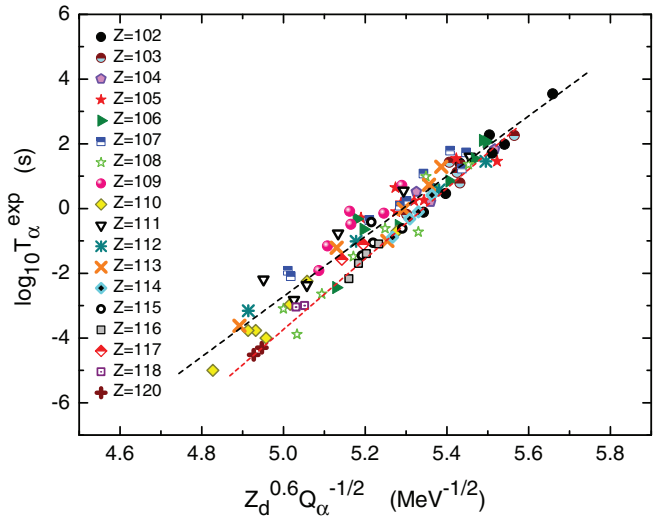

FIG. 6. (Color online) The experimental α half-lives plotted vs $Z_d^{0.6} Q_\alpha^{-1/2}$ for 99 data points. The straight lines represent the results of the linear fits for the (e-e) nuclei and the (e-o, o-e, o-o) nuclei.

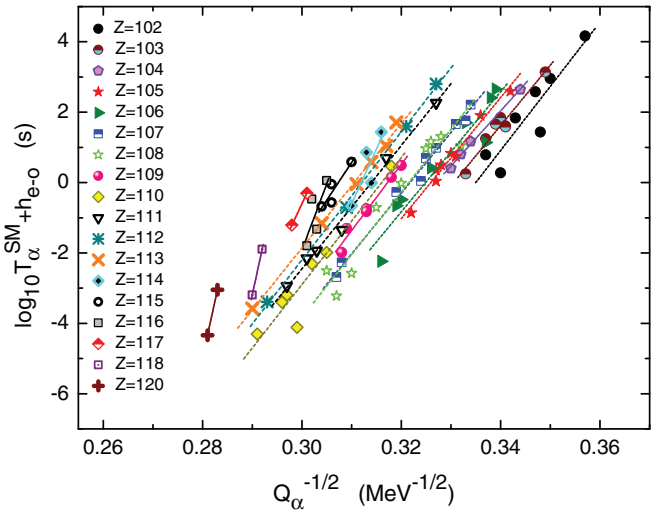

FIG. 7. (Color online) The $\log T_\alpha^{\mathrm{SM}}$ values plus the even-odd correction h_{e-o} plotted vs $Q_\alpha^{-1/2}$ for 99 data points.

in Figs. 3–5 cannot be reproduced by the values of $\log T_\alpha^{\mathrm{SM}}$ in Figs. 7–9 without the even-odd corrections h_{e-o}. With these corrections added, the agreement with experimental data is improved and basic trends in the systematics of data are well reproduced. In comparing Figs. 3–5 and Figs. 7–9 one may conclude the following:

(i) The isotopic lines in Figs. 3 and 4 are not well separated for the data points, while for the calculated SM data points in Figs. 7 and 8 these lines are very well separated.

(ii) The scatter in Figs. 4 and 8 ($Z_d Q_\alpha^{-1/2}$) is less pronounced than that in Figs. 3 and 7 ($Q_\alpha^{-1/2}$). Also the Z_d lines show an approximate constant slope in Figs. 4 and 8.

(iii) When passing from the plot of $\log T_\alpha$ vs $Q_\alpha^{-1/2}$ to the plot of $\log T_\alpha$ vs $Z_d Q_\alpha^{-1/2}$, the all isotopic lines are

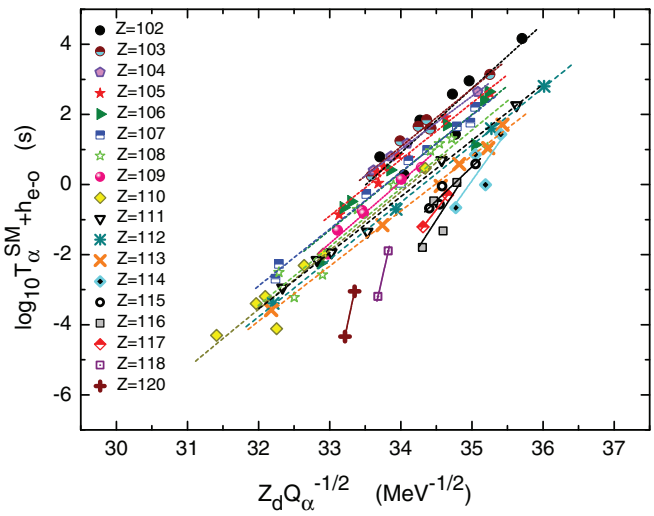

FIG. 8. (Color online) The $\log T_\alpha^{\mathrm{SM}}$ values plus the even-odd correction h_{e-o} plotted vs $Z_d Q_\alpha^{-1/2}$ for 99 data points.

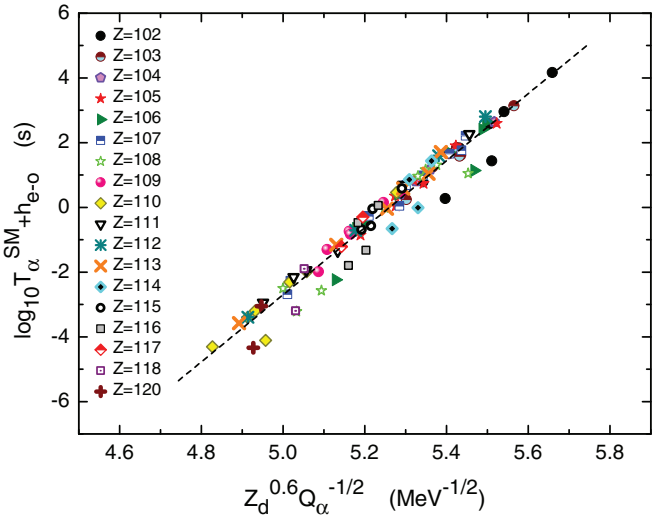

FIG. 9. (Color online) The $\log T_\alpha^{\rm SM}$ values plus the even-odd correction h_{e-o} plotted vs $Z_d^{0.6} Q_\alpha^{-1/2}$ for 99 data points. The straight line represents the result of the linear fit.

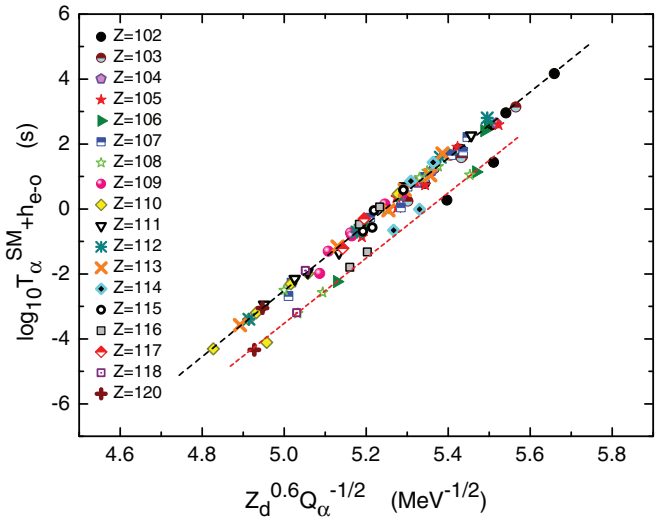

FIG. 10. (Color online) The $\log T_\alpha^{\rm SM}$ values plus the even-odd correction h_{e-o} plotted vs $Z_d^{0.6} Q_\alpha^{-1/2}$ for 99 data points. The straight lines represent the results of the linear fits for the (e-e) nuclei and the (e-o, o-e, o-o) nuclei.

reversed with respect to the magic isotopic line $Z = 108$ (Hs).

(iv) The Brown plot ($\log T_\alpha$ vs $Z_d^{0.6} Q_\alpha^{-1/2}$) in Figs. 5 and 9 which puts all the emitters with different Z values on the same line is very relevant for the systematics of both experimental and calculated α half-lives.

Advanced systematic studies of α-decay properties of SHN have been realized starting from

(i) the R-matrix theory (Thomas-Mang) [39,40],
(ii) the generalization of the Geiger-Nuttall law within the microscopic [41] and macroscopic [42] mechanisms of the charged particle radioactivity,
(iii) different folding [43,44] and mean-field [45] potentials, and
(iv) microscopic calculations of α-half lives within the cluster model with spherical and deformed potentials [35] and the two-center SM [46].

It should to be stressed that our results illustrated graphically in Figs. 5 and 6 and in Figs. 9 and 10 are similar to the ones reported in Refs. [41,42] where the universal line for cluster-decay half-lives was first introduced.

C. Fit formulas for α half-lives

From the single-line fits of the experimental and calculated values of $\log T_\alpha$ vs $Z_d^{0.6} Q_\alpha^{-1/2}$, we obtain two simple formulas for α half-lives:

$$\log T_\alpha^{\rm exp}(s) = 9.68(Z_d^{0.6} Q_\alpha^{-1/2}) - 51.32, \ {\rm rms}^{\rm exp} = 0.51. \tag{9}$$

$$\log T_\alpha^{\rm SM}(s) = 10.36(Z_d^{0.6} Q_\alpha^{-1/2}) - 54.51, \ {\rm rms}^{\rm SM} = 0.39. \tag{10}$$

The straight line in Fig. 5 [see Eq.(9)] represents the single linear fit of 99 data points for SHN. This line is very close to the Brown line [Eq. (B2)] deduced from the data fit of heavy and SHN (known until 1992).

Notice that the $T^{\rm SM}$ values obtained from Eq. (10) are greater than the $T^{\rm exp}$ values obtained from Eq. (9) and ${\rm rms}^{\rm exp} > {\rm rms}^{\rm SM}$.

The α decay involving unpaired nucleons (Z, N) = (e-o, o-e, o-o) always proceeds more slowly than that involving pairs (Z, N) = (e-e). This suggests some "*hindrance*" of α transitions in odd nuclei due to internal selection rules. Therefore, it is interesting to fit the experimental and calculated α half-lives for SHN, separately, with the distinct (Z, N) parities. Doing so, the experimental and calculated points appear to fall on nearly parallel straight lines which represent the best fits of the data, with the lowest rms deviation from the straight line fit as shown in Figs. 6 and 10.

From the two-line fits of experimental and calculated half-lives for (e-e) and (o-e, e-o, o-o) nuclei, respectively, we get

$$\log T_\alpha^{\rm exp}(s) = 10.91\left(Z_d^{0.6} Q_\alpha^{-1/2}\right) - 58.27,$$
$${\rm rms}^{\rm exp} = 0.20, \ \text{for 14 (e-e) nuclei,} \tag{11}$$
$$\log T_\alpha^{\rm exp}(s) = 9.30\left(Z_d^{0.6} Q_\alpha^{-1/2}\right) - 49.20,$$
$${\rm rms}^{\rm exp} = 0.47, \ \text{for 85 (e-o, o-e, o-o) nuclei,} \tag{12}$$
$$\log T_\alpha^{\rm SM}(s) = 10.04\left(Z_d^{0.6} Q_\alpha^{-1/2}\right) - 53.74,$$
$${\rm rms}^{\rm SM} = 0.12, \ \text{for 14 (e-e) nuclei,} \tag{13}$$
$$\log T_\alpha^{\rm SM}(s) = 10.19\left(Z_d^{0.6} Q_\alpha^{-1/2}\right) - 53.46,$$
$${\rm rms}^{\rm SM} = 0.15, \ \text{for 85 (e-o, o-e, o-o) nuclei.} \tag{14}$$

The value ${\rm rms}^{\rm exp} = 0.20$ in the two-line fit [see Eq. (11) and Fig. 10] is lower than the value rms = 0.33 of the single-line plot of Brown (see Ref. [38]). The big ${\rm rms}^{\rm exp}$ value corresponding to Eq. (12) indicates large data errors for old nuclei. The ${\rm rms}^{\rm SM}$ values for (e-e) and (e-o, o-e, o-o) nuclei

[see Eqs. (13) and (14)] are comparable and are lower than the rms^{exp} values [see Eqs. (11) and (12)].

IV. SUMMARY AND OUTLOOK

In summary, we defined and evaluated an approximation scheme that can be used to determine α half-lives of shell stabilized SHN. This scheme takes into account the evolution of the structure in the open shell nuclei and the sensible interplay between the microscopic structure and the reaction mechanism. In general, our estimations for α half-lives agree with the experimental data. Also, the quantitative and qualitative fits to current experimental data and theoretical results are in relatively good accord. The systematics of the α-decay data is very well reproduced by the results of the SMRT.

The influence of different effects and corrections (even-odd, shell closures, resonance scattering, finite size, screening) on α half-lives has been evidenced and plausible explanations for some discrepancies between calculated and experimental α half-lives are given. For the SHN nuclei it is of importance to predict, even roughly, the radioactive properties of unknown species. Such predictions can be made with a fair degree of confidence and this may help in the preparation and identification of new nuclear species in the superheavy region.

Comparison of experimental and calculated α half-lives and their systematics provides insight into the accuracy of modern approaches for the nuclear structure and dynamics of the heaviest nuclei.

ACKNOWLEDGMENTS

We thank Professors Yu. Ts. Oganessian, V. K. Utyonkov, G. Münzenberg, W. Scheid, A. Săndulescu, S. Misicu, and M. Mirea for many stimulating discussions. This work was supported by Contracts No. Idei 068/05.10.2011 and No. PN 09 37 01 02/2009.

APPENDIX A: MATRIX ELEMENTS V_{nm}

The diagonal elements V_{nn} of the potential are given by a sum of nuclear and Coulomb terms:

$$V_{nn}(r) = V_0^{\text{nucl}}(r) + V_0^{\text{Coul}}(r).$$

For the nuclear potential we use the Woods-Saxon parametrization:

$$V_0^{\text{nucl}}(r) = -\frac{V_0}{1+\exp[(r-R_0)/a]},$$

where V_0 is the depth, $R_0 = r_0(A_P^{1/3} + A_D^{1/3})$, with r_0 being a given parameter, while A_P and A_D are the particle and the daughter masses, respectively, and a is the diffuseness.

The Coulomb potential is taken as the usual form:

$$V_0^{\text{Coul}}(r) = \begin{cases} \frac{Z_P Z_D e^2}{2R_c}\left[3 - \left(\frac{r}{R_c}\right)^2\right], & r \leqslant R_c, \\ \frac{Z_P Z_D e^2}{r}, & r > R_c. \end{cases}$$

where e is the electron charge; Z_P and Z_D are the atomic numbers of the particle and the target, respectively; and $R_c = r_c(A_P^{1/3} + A_D^{1/3})$, with r_c being an input parameter.

Also the matrix elements V_{ij} of the coupling Hamiltonian consist of nuclear and Coulomb components. The nuclear component can be generated by changing the daughter radius in the nuclear potential to a dynamical operator,

$$R_0 \to R_0 + \hat{O} = R_0 + \beta_2 R_D Y_{20} + \beta_4 R_D Y_{40},$$

where $R_D = r_0 A_D^{1/3}$, Y_{20} and Y_{40} are the spherical harmonic functions, and β_2, β_4 are the quadrupole and hexadecapole deformation parameters of the deformed target nucleus, respectively. The nuclear coupling term is thus given by

$$V^{\text{nucl}}(r, \hat{O}) = -\frac{V_0}{1+\exp[(r-R_0-\hat{O})/a]}.$$

To obtain the matrix elements of this coupling Hamiltonian, one first looks for the eigenvalues and eigenvectors of the operator. This is done by diagonalizing the matrix with the elements (see [47,48]):

$$\hat{O}_{nm} = \sqrt{\frac{5(2I+1)(2J+1)}{4\pi}}\beta_2 R_D \begin{pmatrix} I & 2 & J \\ 0 & 0 & 0 \end{pmatrix}^2 + \sqrt{\frac{9(2I+1)(2J+1)}{4\pi}}\beta_4 R_D \begin{pmatrix} I & 4 & J \\ 0 & 0 & 0 \end{pmatrix}^2, \quad \text{(A1)}$$

where $I = 2(n-1)$, $J = 2(m-1)$, and Wigner $3j$ symbols are used. Denoting the eigenvalues by ω_k, $k = 1, \ldots, n$, and the components of the eigenvector corresponding to the eigenvalue ω_k by Ω_{ik}, $i = 1, \ldots, p$, the nuclear coupling matrix elements are then given by

$$V_{nm}^{\text{nucl}}(r) = \sum_{k=1}^{p} \Omega_{ik} V^{\text{nucl}}(r, \omega_k)\Omega_{jk} - V_0^{\text{nucl}}(r)\delta_{n,m}. \quad \text{(A2)}$$

The last term in this equation is included to avoid the double counting of the diagonal component.

For the Coulomb interaction, we include terms up to the second order with respect to β_2 and up to the first order with respect to β_4.

With the notations $I = 2(n-1)$ and $J = 2(m-1)$, the Coulomb matrix elements are given by

$$V_{nm}^{\text{Coul}}(r) = \frac{3Z_P Z_D}{5} F_2(r)\sqrt{\frac{5(2I+1)(2m+1)}{4\pi}} \times \left(\beta_2 + \frac{2}{7}\sqrt{\frac{5}{\pi}}\beta_2^2\right)\begin{pmatrix} I & 2 & J \\ 0 & 0 & 0 \end{pmatrix}^2 + \frac{3Z_P Z_D}{9} F_4(r)\sqrt{\frac{9(2I+1)(2J+1)}{4\pi}} \times \left(\beta_4 + \frac{9}{7}\beta_2^2\right)\begin{pmatrix} I & 4 & J \\ 0 & 0 & 0 \end{pmatrix}^2, \quad \text{(A3)}$$

where, for $p = 2$ and $p = 4$,

$$F_n(r) = \begin{cases} \frac{r^p}{R_D^{p+1}}, & r \leqslant R_D, \\ \frac{R_D^p}{r^{p+1}}, & r > R_D. \end{cases}$$

The total coupling matrix element is given by the sum of V_{nm}^{nucl} and V_{nm}^{Coul}.

APPENDIX B: EMPIRICAL FORMULAS

The Geiger-Nuttall law [36] relates the half-life of a radioactive isotope with the energy of the α particle emitted. This was the observation that the experimental values of $\log T_\alpha$ plotted vs $Q_\alpha^{-1/2}$, where Q_α is the α-decay energy, fall on straight lines for the isotopes of a given element. The law also shows that half-lives are exponentially dependent on decay energy, so that short-lived isotopes emit more energetic α particles than long-lived ones. Gamow [49] and independently Gurney and Condon [50] have solved the one-body problem of the α-decay and derived the known Geiger-Nuttall rule from the first principles of quantum mechanics. An explicit functional dependence of the half-time on the energy Q_α and on the proton number of the daughter nucleus Z_d was introduced later in formulations given in Refs. [37,38]. Here we consider two phenomenological formulas. The first one is the Viola-Seaborg formula [37], which reads as

$$\log T_\alpha(s) = (aZ_d + b)Q_\alpha^{-1/2} + (cZ_d + d) + h_{e-o}, \quad \text{(B1)}$$

where Q_α is the decay energy in MeV units; Z_d is the charge number of the daughter nucleus; a, b, c, and d are parameters; and h_{e-o} is an even-odd hindrance term. The parameters used are from Ref. [51]: $a = 1.66175$; $b = -8.5166$; $c = -0.20228$; $d = -33.9069$, $h_{e-e} = 0.0$ ($Z =$ even, $N =$ even); $h_{o-e} = 0.772$ ($Z =$ odd, $N =$ even); $h_{e-o} = 1.066$ ($Z =$ even, $N =$ odd); and $h_{o-o} = 1.114$ ($Z =$ odd, $N =$ odd).

The second one is the Brown formula [38] written as

$$\log T_\alpha(s) = 9.54 Z_d^{0.6} Q_\alpha^{-1/2} - 51.37 + h_{e-o}, \quad \text{(B2)}$$

where the constants are determined from the best linear fit of 119 data points (T_α, Q_α) in a range of Z_d from 74 to 106 for even-even nuclei.

[1] Y. T. Oganessian *et al.*, Phys. Rev. C. **87**, 014302 (2013).
[2] Y. T. Oganessian *et al.*, Phys. Rev. C **79**, 024603 (2009).
[3] Y. T. Oganessian *et al.*, Phys. Rev. C **76**, 011601(R) (2007).
[4] Yu. Oganessian, J. Phys. G **34**, R165 (2007).
[5] Y. T. Oganessian, Pure. Appl. Chem. **78**, 889 (2006).
[6] S. Hofmann *et al.*, Eur. Phys. J. A **14**, 147 (2002).
[7] S. Hofmann and G. Münzenberg, Rev. Mod. Phys. **72**, 733 (2000).
[8] S. Hofmann *et al.*, Nucl. Phys. A **734**, 93 (2004); Z. Phys. A **354**, 229 (1996).
[9] K. Morita *et al.*, Jpn. Phys. Soc. J. **73**, 2593 (2004).
[10] J. Dvorak *et al.*, Phys. Rev. Lett. **100**, 132503 (2008).
[11] P. A. Ellison *et al.*, Phys. Rev. Lett. **105**, 182701 (2010).
[12] Ch. E. Düllmann *et al.*, Phys. Rev. Lett. **104**, 252701 (2010).
[13] H. Haba *et al.*, Phys. Rev. C **83**, 034602 (2011).
[14] J. Piot *et al.*, Phys. Rev. C **85**, 041301 (2012).
[15] I. Dragojevic *et al.*, Phys. Rev. C **79**, 011602(R) (2009).
[16] F. P. Hessberger, Phys. Atom. Nucl. **70**, 1445 (2007); M. Leino and F. P. Hessberger, Nucl. Part. Sci. **54**, 175 (2004).
[17] A. Baran, Z. Łojewski, K. Sieja, and M. Kowal, Phys. Rev. C **72**, 044310 (2005).
[18] P. Roy Chowdhury, C. Samanta, and D. N. Basu, At. Data Nucl. Data Tables **94**, 781 (2008).
[19] V. Y. Denisov and A. A. Khudenko, At. Data Nucl. Data Tables **95**, 815 (2009).
[20] V. Y. Denisov and A. A. Khudenko, Phys. Rev. C **79**, 054614 (2009); **80**, 034603 (2009).
[21] I. Silişteanu and A. I. Budaca, At. Data Nucl. Data Tables **98**, 1096 (2012); Rom. J. Phys. **57**, 493 (2012); **55**, 1088 (2010); **58**, 1198 (2013).
[22] A. I. Budaca and I. Silişteanu, J. Phys.: Conf. Series **413**, 012027 (2013); **337**, 012022 (2012); Rom. Rep. Phys. **63**, 1147 (2011).
[23] D. Bucurescu and N. V. Zamfir, Phys. Rev. C **87**, 054324 (2013).
[24] I. Silişteanu, W. Scheid, and A. Săndulescu, Nucl. Phys. A **679**, 317 (2001).
[25] H. J. Mang, Phys. Rev. **119**, 1069 (1960).
[26] G. Breit, in *Encyclopedia of Physics*, Vol. XLI, *Nuclear Reactions II: Theory*, edited by S. Flugge (Springer-Verlag, Berlin, 1959).
[27] H. Feshbach, Ann. Phys. **5**, 357 (1958).
[28] J. O. Rasmussen, in *Alpha-, Beta- and Gamma-Ray Spectroscopy*, edited by K. Siegbahn (North-Holland, Amsterdam, 1968), Vol. 1, p. 701.
[29] V. Ledoux, M. Rizea, M. Van Daele, G. Vanden Berghe, and I. Silişteanu, J. Comput. Appl. Math. **228**, 197 (2009).
[30] P. Möller, J. Nix, and K. L. Kratz, At. Data Nucl. Data Tables **66**, 131 (1997).
[31] I. Silişteanu and W. Scheid, Phys. Rev. C **51**, 2023 (1995).
[32] A.-T. Kruppa, M. Bender, W. Nazarewicz, P.-G. Reinhard, T. Vertse, and S. Ćwiok, Phys. Rev. C **61**, 034313 (2000).
[33] S. Hofmann, Rom. J. Phys. **57**, 214 (2012).
[34] A. Sobiczewski, Rom. J. Phys. **57**, 506 (2012).
[35] D. Ni and Z. Ren, Phys. Rev. C **80**, 051303 (2009); Nucl. Phys. A **828**, 348 (2009); Rom. J. Phys. **57**, 407 (2012).
[36] H. Geiger and J. M. Nuttall, Philos. Mag. **22**, 613 (1911).
[37] V. E. Viola and G. T. Seaborg, J. Inorg. Nucl. Chem. **28**, 741 (1966).
[38] B. A. Brown, Phys. Rev. C **46**, 811 (1992).
[39] D. S. Delion, *Theory of Particle and Cluster Emission* (Springer-Verlag, Berlin, 2010).
[40] D. S. Delion, A. Săndulescu, and W. Greiner, Phys. Rev. C **69**, 044318 (2004).
[41] C. Qi, F. R. Xu, R. J. Liotta, R. Wyss, M. Y. Zhang, C. Asawatangtrakuldee, and D. Hu, Phys. Rev. C **80**, 044326 (2009).
[42] D. N. Poenaru, R. A. Gherghescu, and W. Greiner, Phys. Rev. C **83**, 014601 (2011).
[43] K. P. Santhosh, B. Priyanka, and M. S. Unnikrishnan, Phys. Rev. C **85**, 034604 (2012).
[44] K. P. Santhosh Jayesh, G. Joseph, and B. Priyanka, J. Phys. G: Nucl. Part. **38**, 075101 (2011).
[45] B. K. Sahu *et al.*, Int. J. Mod. Phys. E **20**, 2217 (2011).

[46] A. Săndulescu, M. Mirea, and D. S. Delion, Europhys. Lett. **101**, 62001 (2013).
[47] M. W. Kermode and N. Rowley, Phys. Rev. C **48**, 2326 (1993).
[48] K. Hagino, N. Rowley, and A. T. Kruppa, Comp. Phys. Commun. **123**, 143 (1999).
[49] G. Gamow, Z. Phys. **51**, 204 (1928).
[50] R. W. Gurney and E. U. Condon, Nature (London) **122**, 439 (1928).
[51] A. Sobiczewski, Z. Patyk, and S. Cwiok, Phys. Lett. B **224**, 1 (1989).